Journal of Alloys and Compounds 509 (2011) 3587–3591

Contents lists available at ScienceDirect

Journal of Alloys and Compounds

journal homepage: www.elsevier.com/locate/jallcom

Synthesis of nanocrystalline nickel–zinc ferrite ($Ni_{0.8}Zn_{0.2}Fe_2O_4$) thin films by chemical bath deposition method

D.K. Pawar[a], S.M. Pawar[b], P.S. Patil[c], S.S. Kolekar[a,*]

[a] Department of Chemistry, Shivaji University, Kolhapur 416 004 (M.S.), India
[b] Department of Materials Science and Engineering, Chonnam National University, 500 757,South Korea
[c] Department of Physics, Shivaji University, Kolhapur 416 004 (M.S.), India

ARTICLE INFO

Article history:
Received 21 July 2010
Received in revised form 9 December 2010
Accepted 12 December 2010
Available online 21 December 2010

Keywords:
Nickel–zinc ferrite
Chemical bath deposition
Flakes like morphology
X-ray diffraction
Cyclic voltammetry

ABSTRACT

The nickel–zinc ferrite ($Ni_{0.8}Zn_{0.2}Fe_2O_4$) thin films have been successfully deposited on stainless steel substrates using a chemical bath deposition method from alkaline bath. The films were characterized by X-ray diffraction (XRD), Fourier transform infrared spectroscopy (FTIR), scanning electron microscopy (SEM), static water contact angle and cyclic voltammetry measurements. The X-ray diffraction pattern shows that deposited $Ni_{0.8}Zn_{0.2}Fe_2O_4$ thin films were oriented along (3 1 1) plane. The FTIR spectra showed strong absorption peaks around 600 cm^{-1} which are typical for cubic spinel crystal structure. SEM study revealed compact flakes like morphology having thickness ~1.8 μm after air annealing. The annealed films were super hydrophilic in nature having a static water contact angle (θ) of 5°.The electrochemical supercapacitor study of $Ni_{0.8}Zn_{0.2}Fe_2O_4$ thin films has been carried out in 6 M KOH electrolyte.

The values of interfacial and specific capacitances obtained were 0.0285 F cm^{-2} and 19 F g^{-1}, respectively.

1. Introduction

The nanocrystalline ferrite thin films with spinel cubic structure have been subject of extensive investigation because of their potential applications in high-density magneto-optic recording devices, color imaging, bioprocessing, magnetic refrigeration and ferrofluids [1–3]. In particular, nanocrystalline nickel–zinc ferrite thin films are of great interest at microwave frequencies not only due to properties like high resistivity and lower losses but also because they can be easily prepared at lower annealing temperature [4–10]. Nickel–zinc ferrite thin films can also be used as non-reciprocal ferrite components on a microwave monolithic integrated circuit (MMIC) based on GaAs and as back layers to improve recording performances at high frequencies [11,12]. Ni–Zn ferrite is a type of mixed spinel in which tetrahedral (A) sites are occupied by Zn^{2+} and Fe^{3+} ions, whereas the octahedral (B) sites are occupied by Ni^{2+} and Fe^{3+} in the cubic spinel lattice. These two anti-parallel sublattices form a ferromagnetic structure, in which $Ni^{2+}$and $Fe^{3+}$are coupled by super exchange interactions through the O^{2-} ions. At present, bulk Ni–Zn ferrite components employed in discrete devices at microwave frequencies are not compatible with the rapid developments of electronic applications towards miniaturation, high density, integration, and multifunction. Thus, more attention has been attracted to solve these difficulties in performing the required miniaturization for complex devices [13]. Ni–Zn ferrite films may play an important role in facilitating the design and fabrication of devices such as micro-inductors, micro-transformers, and microwave nonreciprocal devices [14]. The ferrite thin films incorporated into magnetic integrated circuits are expected to replace the current surface mounting modules in the near future. The successful growth of magnetic Ni–Zn ferrite films is an important step towards their future incorporation as inductors and transformers into integrated circuits operating at high frequency. Several attempts have been made by researchers to deposit Ni–Zn ferrite films by a variety of techniques including alternative sputtering technology [15], spin–spray plating [16], sol–gel method [17,18], pulsed laser deposition [19–21], spray and spin deposition techniques [22–25]. However, most of them cannot be economically applied on a large scale because they require high vacuum system, complicated experimental steps, and high reaction temperatures. Additionally, the higher coercivity in Ni–Zn ferrite films compared with bulk materials, which leads mainly to eddy current loss, has become a barrier in the way of applications. Due to the drawbacks of physical methods, recently much emphasis has been put on the chemical processes for the preparation of advanced inorganic materials such as spinel type oxides [26], pervoskite-type oxides [27], nanotubes, nanowires [28] and nanodots with quantum size effects. These low cost processes have used environmentally benign condi-

* Corresponding author. Tel.: +91 231 2609163; fax: +91 231 2692333.
E-mail address: kolekarss2003@yahoo.co.in (S.S. Kolekar).

0925-8388/$ – see front matter © 2010 Elsevier B.V. All rights reserved.
doi:10.1016/j.jallcom.2010.12.079

tions. Chemical methods are simple, economic and convenient for the deposition of metallic chalcogenide thin films. The preparative parameters such as concentration, pH, nature of the complexing agent, bath temperature, etc. are easily controllable [29]. The ferrite thin films were mostly prepared at temperatures of more than several hundred degrees [30]. It is well known that deposition at high temperature is critical and affects the reproducibility and the quality of the films and suffers additionally from the environmental pollution due to the evolution of toxic gases during the deposition [31]. The low temperature deposition avoids oxidation and corrosion of metallic substrates. Chemical methods results into pinhole free and uniform deposition. Therefore, these chemical processes are important for the preparation of the nanocrystalline thin films. Such processes include electrochemical deposition, sol–gel dip coating, chemical vapour deposition, chemical solution method, etc. Till date, there is no report available on the synthesis of Ni–Zn ferrite thin films using low temperature chemical bath deposition method.

In the present research paper, we report, the synthesis of single-phase spinel $Ni_{0.8}Zn_{0.2}Fe_2O_4$ thin films by chemical bath deposition method (CBD) at low temperature (328 K). The deposited films have been characterized using X-ray diffraction (XRD), Fourier transform infrared (FT-IR) spectroscopy, scanning electron microscopy (SEM), static water contact angle measurements and cyclic voltammetry measurements for supercapacitor application.

2. Experimental

2.1. Preparation of $Ni_{0.8}Zn_{0.2}Fe_2O_4$ thin films

Preparation of $Ni_{0.8}Zn_{0.2}Fe_2O_4$ thin films by CBD method was based on the heating of alkaline bath of combined chloride salts of nickel(II), zinc(II) and iron(II) metals. Combined Ni^{2+}, Zn^{2+} and Fe^{2+} ions were used as source of cations and to make it alkaline, aqueous ammonia solution was added to adjust the pH of the solution (source of oxygen atoms) as well as the complexing agent. Concentration ratio of the Ni^{2+}, Zn^{2+} to Fe^{2+} was kept constant at 1:2. All solutions were prepared immediately before deposition by dissolving required amounts of analytical reagents grade (AR grade) chemicals in double distilled water. The pH of the resultant solution was optimized to 9.40. The stainless steel was used as the substrate. Before using stainless steel substrates in the chemical bath, they were polished by smooth polish paper (zero fine grade) and cleaned with doubled distilled water. In order to remove the oily substance from the surface, cleaned substrates were etched in 10% H_2SO_4 for 2 min and finally ultrasonically cleaned with double distilled water and dried with hot air. These cleaned substrates were immersed in the bath and the bath was heated. When the bath attained the temperature of 328 K, the precipitation was started. During the precipitation, heterogeneous reaction occurred on the substrate and deposition of $Ni_{0.8}Zn_{0.2}Fe_2O_4$ took place on the substrate. The film formation started at about 35 min and completed nearly at 150 min. After the deposition, thin film deposited substrates were removed from the bath and washed with deionised water followed by drying under hot air flow. However, inclusion of metal hydroxide is also possible due to the aqueous alkaline nature of the bath [32]; the $Ni_{0.8}Zn_{0.2}Fe_2O_4$ films were air annealed at 723 K for 6 h to remove the surface hydroxides. The annealed thin film has average film thickness of 1.8 μm.

2.2. Characterization techniques

The average film thickness of the annealed film was measured by thickness profiler AMBIOS (XP-1). The structural analysis of the $Ni_{0.8}Zn_{0.2}Fe_2O_4$ film was carried out using X-ray diffraction (XRD) within the range 20–60° on computer controlled Philips PW-3710 using Cr Kα (λ = 2.2897 Å) radiations. The Fourier transform infrared (FTIR) spectrum of the sample was recorded using PerkinElmer, FTIR Spectrum one unit. The microstructure of the film was observed using scanning electron microscopy (JEOL-JSM 6360, Japan). The wettability of the film was evaluated by measuring the contact angle (θ) of a water droplet of 10 μl placed on the film surface using the contact angle meter equipped with a CCD camera (Ramehart Instrument Co., USA) at an ambient temperature. The static water contact angles were measured at four different positions for each sample, and the average value was adopted as the contact angle. The cyclic voltammetry measurement was carried out for supercapacitor application.

3. Results and discussion

3.1. Film formation and reaction mechanism

The Ni–Zn ferrite thin films deposited by CBD method were uniform and well adherent to the substrates. When the process is considered in a qualitative way, the film growth is dominated by three periods: (i) nucleation or incubation period, during which the various chemical equilibriums and reactions are established in the bath. (ii) The growth period during which the film thickness has an approximately linear variety with deposition time. At the moment, the ionic product (IP) of the solution exceeds the solubility product (SP), and the solution reaches a maximum degree of super saturation (S = degree of super saturation = IP/SP), which consequently leads to the growth of nuclei and deposition of the film. (iii) A terminal step where the reagent becomes depleted and the film growth begins to slow and eventually stops. For deposition of $Ni_{0.8}Zn_{0.2}Fe_2O_4$ thin film, aqueous solution consisting of nickel(II) chloride, zinc(II) chloride and iron(II) chloride salts as a source of Ni^{2+}, Zn^{2+} and Fe^{2+} ions was used. Aqueous ammonia solution was used as complexing agent to adjust the pH (9.40) of the solution. The concentration ratio of Ni^{2+}, Zn^{2+} and Fe^{2+} ions in the bath was kept constant as 1:2. The ultrasonically cleaned substrate was immersed in deposition bath consisting of alkaline nickel(II) chloride, zinc(II) chloride and iron(II) chloride solution so as to get nickel, zinc and iron hydroxides adsorbed onto the substrate. This can be represented by the following reactions:

$$NiCl_2 + 2NH_4OH \rightarrow Ni(OH)_2 + 2NH_4Cl \quad (1)$$

$$ZnCl_2 + 2NH_4OH \rightarrow Zn(OH)_2 + 2NH_4Cl \quad (2)$$

$$FeCl_2 + 2NH_4OH \rightarrow Fe(OH)_2 + 2NH_4Cl \quad (3)$$

In an aqueous alkaline bath, oxidation of ferrous hydroxide produces iron oxyhydroxide (geothite) represented by following reaction mechanism [33].

$$Fe(OH)_2 \rightarrow Fe(OH)_3 \rightarrow Fe(OH)_3aq \rightarrow FeO_m(OH)_{3-2m} \rightarrow \alpha/\gamma - FeOOH \quad (4)$$

When the deposited film was annealed at 723 K, it crystallized to nickel–zinc ferrite with cubic spinel phase by removing all hydroxide content.

$$Ni(OH)_2 + Zn(OH)_2 + 3FeOOH \rightarrow NiZnFe_2O_4 + 2H_2O \uparrow \quad (5)$$

3.2. Structural analysis

Fig. 1 shows the typical X-ray diffraction patterns of as-deposited and annealed $Ni_{0.8}Zn_{0.2}Fe_2O_4$ thin films deposited on stainless steel substrate, respectively. The as-deposited thin film shows (3 1 1) diffraction peak with low crystallinity (Fig. 1(a)). The as-deposited film was annealed at 723 K for 6 h for conversion of nickel, zinc and iron hydroxide to $Ni_{0.8}Zn_{0.2}Fe_2O_4$. The XRD pattern of annealed film (Fig. 1(b)) revealed the enhancement in crystallinity after air annealing. The crystal structure of $Ni_{0.8}Zn_{0.2}Fe_2O_4$ was cubic spinel (JCPDS card no: 08-0234). The $Ni_{0.8}Zn_{0.2}Fe_2O_4$ film was oriented along (3 1 1) plane, other orientations corresponding to (1 1 1) and (2 2 0) planes were also present with relatively lower intensities compared to that of (3 1 1) plane. The crystallite size (D = 29.80 nm) is calculated using Scherrer's formula [34],

$$D = \frac{0.9\lambda}{\beta \cos\theta} \quad (6)$$

where D is the crystallite size, β is the broadening of diffraction line measured at half of its maximum intensity (FWHM) and λ is

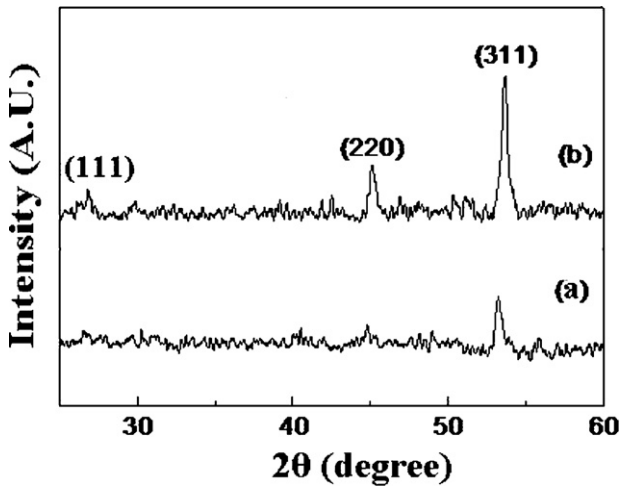

Fig. 1. X-ray diffraction patterns of (a) as-deposited $Ni_{0.8}Zn_{0.2}Fe_2O_4$ thin film and (b) annealed $Ni_{0.8}Zn_{0.2}Fe_2O_4$ thin film.

the X-ray wavelength (2.2897 Å). While calculating crystallite size, instrumental broadening is corrected using single crystal silicon line broadening.

3.3. FTIR studies

The FTIR absorption spectra of the as-deposited and annealed $Ni_{0.8}Zn_{0.2}Fe_2O_4$ thin films are shown in Fig. 2. As-deposited film shows (Fig. 2(a)) absorption bands at 573, 1020, 1638 cm^{-1} attributed for stretching vibration of tetrahedral group, lepidocrocite formation and nitrogen from unconsumed reagent form N–O bond. Fig. 2(b) shows annealed $Ni_{0.8}Zn_{0.2}Fe_2O_4$ thin films has intense peaks at 586 cm^{-1} recognized to the stretching vibration of tetrahedral groups Fe^{3+} O^{2-} of spinel ferrites [35]. Absorption bands at 1020 cm^{-1} confirmed that least amount of lepidocrocite was present after annealing. Due to annealing it was observed that intensity of N–O bond is decreased at 1638 cm^{-1}.

3.4. Surface morphological studies

Fig. 3(a)–(c) shows SEM images of as-deposited and annealed $Ni_{0.8}Zn_{0.2}Fe_2O_4$ thin films deposited on stainless steel substrate.

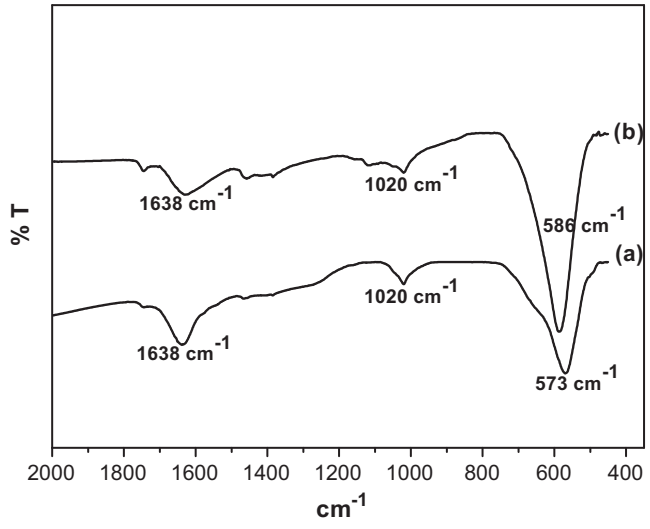

Fig. 2. FTIR spectrum of (a) as-deposited $Ni_{0.8}Zn_{0.2}Fe_2O_4$ thin film and (b) annealed $Ni_{0.8}Zn_{0.2}Fe_2O_4$ thin film.

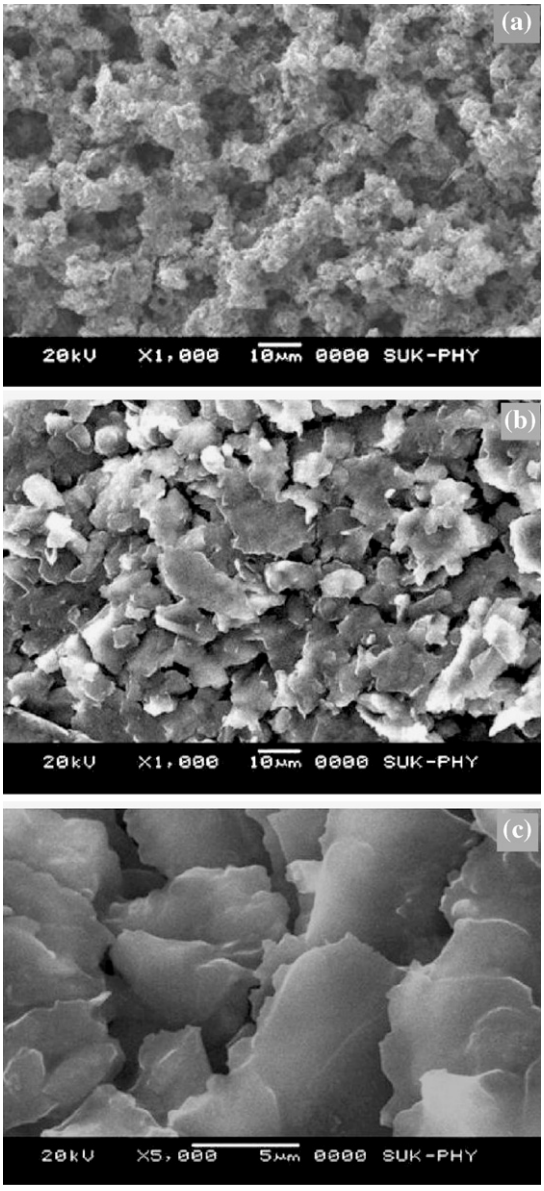

Fig. 3. Scanning electron microscope images of (a) as-deposited $Ni_{0.8}Zn_{0.2}Fe_2O_4$ thin film, (b) annealed $Ni_{0.8}Zn_{0.2}Fe_2O_4$ thin film and (c) annealed $Ni_{0.8}Zn_{0.2}Fe_2O_4$ thin film at 5000× magnification. Inset shows cross sectional SEM image of annealed $Ni_{0.8}Zn_{0.2}Fe_2O_4$ thin film.

As seen from figures, the as-deposited thin film shows connected porous morphology with few voids. The lepidocrocite formation is clearly observed. After annealing it was converted into compact flakes like morphology. There was a significant change in the microstructure of as-deposited and annealed $Ni_{0.8}Zn_{0.2}Fe_2O_4$ thin films. The Fig. 3(c) at higher magnification provides immense evidence that $Ni_{0.8}Zn_{0.2}Fe_2O_4$ thin films has smooth flakes like morphology. Inset, Fig. 3(c) shows that, the thickness of thin film was nearly 1.8 μm.

3.5. Static water contact angle measurements

The influence of surface microstructure on the wetting properties of the as-deposited and annealed $Ni_{0.8}Zn_{0.2}Fe_2O_4$ thin films was demonstrated by the investigation of static water contact angle measurements. An optical microscope lens and a CCD camera were employed herein to take images of the water droplet. Fig. 4(a) and (b) shows static water contact angle of (a) as

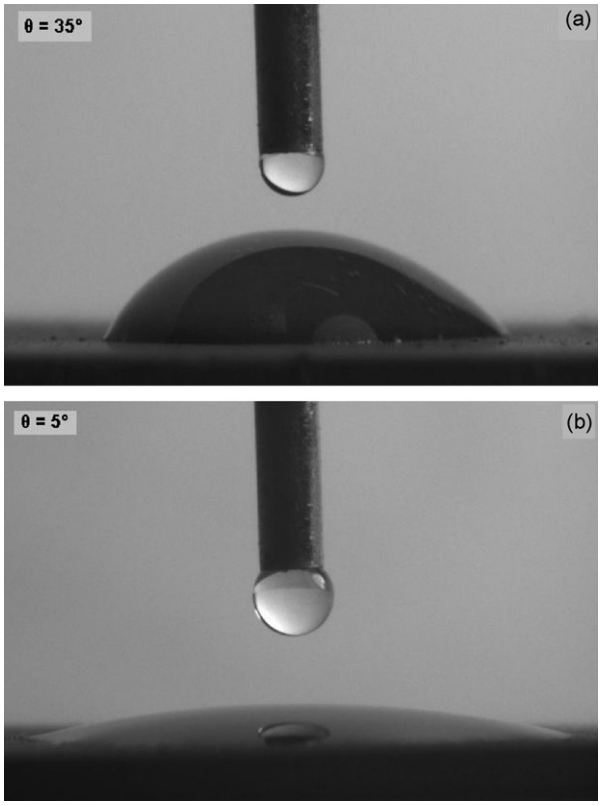

Fig. 4. Static water contact angle of (a) as-deposited $Ni_{0.8}Zn_{0.2}Fe_2O_4$ thin film and (b) annealed $Ni_{0.8}Zn_{0.2}Fe_2O_4$ thin film.

deposited $Ni_{0.8}Zn_{0.2}Fe_2O_4$ thin film, (b) annealed $Ni_{0.8}Zn_{0.2}Fe_2O_4$ thin film. As shown in Fig. 4(a), the as-deposited $Ni_{0.8}Zn_{0.2}Fe_2O_4$ thin film having porous morphology shows static water contact angle of 35°, whereas the annealed $Ni_{0.8}Zn_{0.2}Fe_2O_4$ thin film (Fig. 4(b)) having compact flakes like surface morphology shows static water contact angle of 5°. The as-deposited thin film was hydrophilic ($10^\circ < \theta < 90^\circ$) whereas the annealed thin film was super hydrophilic ($\theta < 10^\circ$) in nature. It shows that the wettability of the surface against water was depending on the surface morphology.

3.6. Supercapacitive studies

The chemically deposited nickel–zinc ferrite ($Ni_{0.8}Zn_{0.2}Fe_2O_4$) thin film was an oxide material used in electrochemical supercapacitor application. In order to increase the energy and power densities, extensive research on metal oxide electrodes and electrolytes in supercapacitor has been carried out. Metal oxides show pseudo-capacitance due to the faradic reactions between the solid material and the electrolyte which is voltage dependent. There is a continuously variable degree of oxidation/reduction, leading to the capacitor behavior. The hydrated nanocrystalline nickel–zinc ferrite (oxide) material exhibits pseudocapacitance in solutions of alkali salts as KOH. During charging, electrons are adsorbed at metal and oxidation state of the metal decreases, whereas, while discharging, desorption of electrons, increases the oxidation state of the metal. This redox processes at the electrode interface are highly reversible and responsible for nickel–zinc ferrite thin film performing as electrochemical supercapacitor. The supercapacitive performance was tested by means of cyclic voltammetry technique. The electrolytes used in the supercapacitors must have a maximum possible decomposition voltage, and broad range of potentials of electrochemical stability. The resistance of the supercapacitor cell

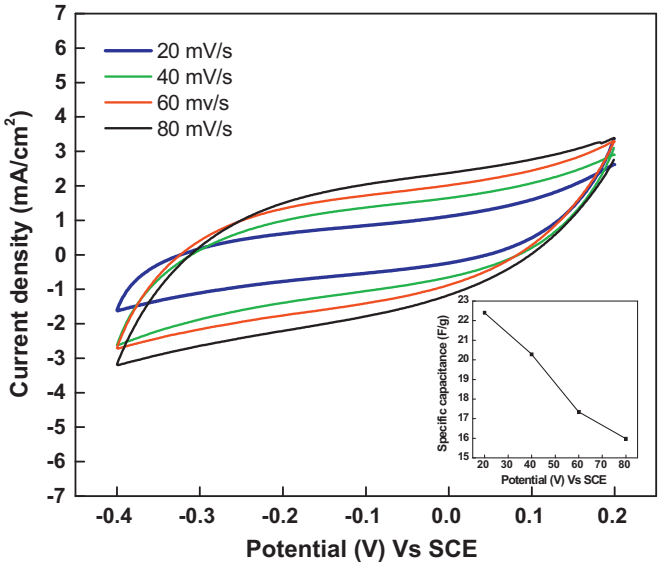

Fig. 5. Cyclic voltammograms of annealed $Ni_{0.8}Zn_{0.2}Fe_2O_4$ thin film in 6 M KOH with different scan rates. Inset shows plot of specific capacitance with scan rate.

is dependent on the resistivity of the electrolyte and size of the ions from the electrolyte that diffuse into and out of the pores of the electrode particles. Organic electrolytes have a higher resistance, but the subsequent power reduction is usually offset by the gain in higher cell voltage. This is usually not a problem for an aqueous electrolyte, such as potassium hydroxide, sodium hydroxide, or sulphuric acid, with the resistivity of 1–2 Ωcm. The aqueous electrolytes are cheaper, easier to purify and have a lower resistance, but they limit the cell voltage to typically 1 V, thereby limiting the maximum achievable power [36]. In the present case, the aqueous 6 M KOH electrolyte was tested for $Ni_{0.8}Zn_{0.2}Fe_2O_4$ thin films. Fig. 5 shows typical C–V curves for different scan rates i.e. 20, 40, 60, 80 mV s^{-1} within the potential range of +200 to −400 mV vs. SCE in KOH electrolyte. The capacitance '*C*' was calculated from the relation:

$$C = \frac{I}{dV/dt} \tag{7}$$

where '*I*' is the average current in amperes and dV/dt is the scan rate in mV s^{-1}. The specific capacitance (F g^{-1}) of the electrode is obtained by dividing the capacitance by the weight and the interfacial capacitance is calculated by dividing the capacitance by the area of the electrode. It is seen that the cyclic voltammograms are almost rectangular and symmetrical also at higher scan rate. This indicates that the oxidation and reduction processes at the electrode interface were highly reversible. From the graph (inset), it is observed that the specific capacitance decreases with increase in scan rate. The decrease in capacitance at higher scan rates is attributed to the presence of inner active sites, which cannot involve in the redox transitions completely, probably due to the diffusion effect of proton within the electrode [37]. The decreasing trend of the capacitance suggests that the parts of the surface of electrode are inaccessible at high charging–discharging rate. Hence, the specific capacitance obtained at the slowest scan rates is believed to be close to that of full utilization of the electrode material. The value of interfacial and specific capacitances obtained were 0.0285 F cm^{-2} and 19 F g^{-1}, respectively.

4. Conclusions

We have successfully synthesized nickel–zinc ferrite ($Ni_{0.8}Zn_{0.2}Fe_2O_4$) thin films on stainless steel substrates using

a low temperature chemical bath deposition method. The X-ray diffraction studies confirmed that the chemically deposited $Ni_{0.8}Zn_{0.2}Fe_2O_4$ thin films are cubic spinel crystal structures. The FTIR spectra showed strong absorption peak around 600 cm^{-1} which is typical for cubic spinel crystal structure. SEM study of the film revealed compact flakes like morphology. The as-deposited and annealed $Ni_{0.8}Zn_{0.2}Fe_2O_4$ thin films showed hydrophilic and super hydrophilic behavior, respectively, depending on the surface morphologies. The value of interfacial and specific capacitances obtained is 0.0285 F cm^{-2} and 19 F g^{-1}, respectively.

Acknowledgements

The authors acknowledge the DST-FIST, UGC-SAP facilities, Department of Chemistry, as well as Department of Physics, Shivaji University, Kolhapur.

References

[1] Z.L. Wang, in: Z.L. Wang (Ed.), Characterization of Nanophase Materials, vol. 1, Wiley, Germany, 2000.
[2] E.S. Murdock, R.F. Simmons, R. Davidson, IEEE Trans. Magn. 28 (1992) 3078–3083.
[3] F. Bodker, S. Morup, S. Linderoth, Phys. Rev. Lett. 72 (1994) 282–285.
[4] D. Ravinder, V.K. Kumar, A.V. Ramana Reddy, Mater. Lett. 57 (2003) 4162–4164.
[5] T.H. Hai, H.T. Van Bich, T.C. Phong, M. Abe, Phys. B: Condens. Matter 327 (2003) 194–197.
[6] Y. Shimada, N. Matsushita, M. Abe, K. Kondo, T. Chiba, S. Yoshida, J. Magn. Magn. Mater. 278 (2004) 256–262.
[7] J. Neamtu, N.P. Pogrion, Proc. ICF-8, Kyoto and Tokyo, Japan, 2000.
[8] M. Abe, T. Itoh, Q. Zhang, S. Kurozumi, IEEE Trans. Magn. 32 (1996) 4183–4185.
[9] P. Samarasekara, R. Rani, F.J. Cadieu, S.A. Shaheen, J. Appl. Phys. 79 (1996) 5425–5427.
[10] S.A. Oliver, C. Vittoria, IEEE Trans. Magn. 30 (1991) 4933–4935.
[11] Y. Kitamoto, M.H. Kim, S. Kantake, M. Abe, M. Naoe, IEEE Trans. Magn. 33 (1997) 3085–3087.
[12] M. Abe, T. Itoh, Y. Tamaura, Y. Goto, M. Gomi, IEEE Trans. Magn. MAG 23 (1997) 3736–3738.
[13] S. Hashi, N. Takada, K. Nishimura, O. Sakurada, S. Yanase, Y. Okazaki, M. Inoue, IEEE Trans. Magn. 41 (2005) 3487–3489.
[14] H.L. Glass, Proc. IEEE 76 (1988) 151–158.
[15] J.H. Gao, Y.T. Cui, Z. Yang, Mater. Sci. Eng. B 110 (2004) 111–114.
[16] N. Matsushita, C.P. Chong, T. Mizutani, M. Abe, IEEE Trans. Magn. 38 (2002) 3156–3158.
[17] F. Liu, C. Yang, T. Ren, A.Z. Wang, J. Yu, L. Liu, J. Magn. Magn. Mater. 309 (2007) 75–79.
[18] N. Xiao-liang, L. Zhong-wen, Y. Zhong, S. Ke, L. Le-zhong, Trans. Nonferrous Met. Soc. China 17 (2007) 854–857.
[19] P.C. Dorsey, B.J. Rappoli, K.S. Grabowski, P. Lubitz, D.B. Chrisey, J.S. Horwitz, J. Appl. Phys. 81 (1997) 6884–6891.
[20] R.G. Welch, J. Neamtu, M.S. Rogalski, S.B. Pahner, Solid State Commun. 97 (1996) 355–359.
[21] O.F. Caltun, J. Optoelectron. Adv. Mater. 7 (2005) 739–744.
[22] A. Takayama, M. Okuya, S. Kaneko, Solid State Ionics 172 (2004) 257–260.
[23] Z. Beji, S. Ammar, L.S. Smiri, M.J. Vaulay, F. Herbst, B. Gallas, F. Fievet, J. Appl. Phys. 103 (2008) 07E744 (1–3).
[24] N. Gupta, A. Verma, S. Kashyap, D. Dube, J. Magn. Magn. Mater. 308 (2007) 137–142.
[25] C.M. Fu, H.S. Hsu, Y.C. Chao, J. Appl. Phys. 93 (2003) 7127–7129.
[26] S.G. Kandalkar, J.L. Gunjakar, C.D. Lokhande, Appl. Surf. Sci. 254 (2008) 5540–5544.
[27] C.D. Lokhande, T.P. Gujar, V.R. Shinde, R.S. Mane, S.H. Han, Electrochem. Commun. 9 (2007) 1805–1809.
[28] L. Vayssieres, Adv. Mater. 15 (2003) 464–466.
[29] R.S. Mane, C.D. Lokhande, Mater. Chem. Phys. 65 (2000) 1–31.
[30] S.H. Yu, M. Yoshimura, Adv. Funct. Mater. 12 (2002) 9–15.
[31] S.D. Sartale, C.D. Lokhande, J. Electroceram. 15 (2005) 35–44.
[32] C.D. Lokhande, P.S. Patil, H. Tributsch, A. Ennaoui, Sol. Energy Mater. Sol. Cells 55 (1998) 379–393.
[33] A.A. Olowe, J.M.R. Genin, Corros. Sci. 32 (1991) 965–984.
[34] P. Scherrer, Gottinger Nachrichten 2 (1918) 98–100.
[35] M. Gotic, I. Czako-Nagy, S. Popovic, S. Music, Philos. Magn. Lett. 78 (1998) 193–201.
[36] R. Kotz, M. Carlen, Electrochim. Acta 45 (2000) 2483–2498.
[37] V. Subramanian, S.C. Hall, P.H. Smith, B. Rambabu, Solid State Ionics 175 (2004) 511–515.